J. theor. Biol. (2001) **213,** 315–331
doi:10.1006/jtbi.2001.2385, available online at http://www.idealibrary.com on IDEAL®

A Cellular Automaton Model of Early Tumor Growth and Invasion*: The Effects of Native Tissue Vascularity and Increased Anaerobic Tumor Metabolism

Aalpen A. Patel†‡, Edward T. Gawlinski§, Susan K. Lemieux‖ and Robert A. Gatenby¶

†*Department of Interventional Radiology, M.D. Anderson Cancer Center,* 1515 *Holcombe Boulevard, Box* 57, *Houston, TX* 77030, *U.S.A.*, §*Department of Physics, Temple University,* 1900 *North* 13*th Street, Barton Hall* 009-00, *Philadelphia, PA* 19122-6082, *U.S.A.*, ‖*Department of Radiology, West Virginia University, P.O. Box* 9235, *Morgantown, WV* 26506-9235, *U.S.A., and* ¶*Department of Radiology, University of Arizona, College of Medicine,* 1501 *North Campbell Avenue, Tucson, AZ* 85724-5067, *U.S.A.*

(*Received on* 17 *October* 2000, *Accepted in revised form on* 22 *July* 2001)

A hybrid cellular automaton model is described and used to simulate early tumor growth and examine the roles of host tissue vascular density and tumor metabolism in the ability of a small number of monoclonal transformed cells to develop into an invasive tumor. The model incorporates normal cells, tumor cells, necrotic or empty space, and a random network of native microvessels as components of a cellular automaton state vector. Diffusion of glucose and H^+ ions (the latter largely resulting from the tumor's excessive reliance on anaerobic metabolism) to and from the microvessels, and their utilization or production by cells, is modeled through the solution of differential equations. In this way, the cells and microvessels affect the extracellular concentrations of glucose and H^+ which, in turn, affect the evolution of the automaton. Simulations of the model demonstrate that: (i) high tumor H^+ ion production is favorable for tumor growth and invasion; however for every H^+ ion production rate, there exists a range of optimal microvessel densities (leading to a local pH favorable to tumor but not to normal cells) for which growth and invasion is most effective, (ii) at vascular densities below this range, both tumor and normal cells die due to excessively low pH, (iii) for vascular densities above the optimal range the microvessel network is highly efficient at removing acid and therefore the tumor cells lose their advantage over normal cells gained by high local H^+ concentration. While significant spatial gradients of glucose formed, no regions of detrimentally poor glucose perfusion (for either cell type) were observed, regardless of microvessel density. Depending on metabolic phenotype, a variety of tumor morphologies similar to those clinically observed were realized in the simulations. Lastly, a sharp transition (analogous to that of the adenoma–carcinoma sequence) between states of initial tumor confinement and efficient invasiveness was observed when H^+ production reached a critical value.

* First in a series of papers.

‡ Corresponding author. Current address: University of Pennsylvania School of Medicine, Hospital of the University of Pennsylvania, Department of Vascular Interventional Radiology, One Silverstein, 3400 Spruce Street, Philladelphia, Pa. 19104. E-mail: patela@oasis.rad.upenn.edu

0022–5193/01/230315 + 17 $35.00/0

Introduction

In an earlier paper (Gatenby & Gawlinski, 1996) we presented an acid-mediated tumor invasion hypothesis (AMTIH) wherein microenvironmental changes at the tumor–host interface caused by altered metabolism in transformed cells (accelerated uptake of glucose due to increased reliance on glycolysis) lead to excess acid production, thus facilitating tumor invasion. In that paper, we also formulated a reaction-diffusion model of the AMTIH that recapitulated a number of features of actual tumor growth, namely growth rate, morphology and crossover from benign to malignant states. Motivated by the need for a model of accurate microscopic fidelity, Patel *et al.* (1998) formulated a model of the AMTIH using a cellular automaton (Wolfram, 1986; Ermentrout & Edelstein-Keshet, 1993). Features of both model- realizations of the hypothesis are grounded on observations first described by Warburg (1930) that tumor cells preferentially convert glucose and other substrate to lactic acid, even under aerobic conditions, resulting in a several fold increase in glucose uptake and lactic acid production in tumor cells versus normal tissue, an increase so marked that it is now routinely used for diagnostic imaging of many types of tumors (Yonekura *et al.*, 1982; Hawkins *et al.*, 1992; Jabour *et al.*, 1993).

Concurrent with this increase of glucose consumption is the up-regulation of the Na^+/H^+ antiport system (Bierman *et al.*, 1987; Kaplan & Boron, 1994). The resulting net increase in tumor intracellular pH leads to normalization and, therefore, to a decrease in extracellular pH by about 0.5 pH units compared to normal tissue (Griffith, 1991; Casciari *et al.*, 1992; Stubbs *et al.*, 1994; Gillies *et al.*, 1994; Martin & Jain, 1994). While some investigators have attributed this increased reliance on glycolysis to the existence of a compromised tumor blood supply leading to poor O_2 perfusion of tumor tissue (Vaupel *et al.*, 1989), others have found evidence that it is a phenotypical consequence of transformation (Smith, 2000).

Because the reaction-diffusion model of the AMTIH predicts the degree to which excess hydrogen ions in the tumor interstitium diffuse into the surrounding tissue, it also predicts the extent of the zone of altered interstitial pH found at the tumor–host interface. This microenvironment is harmful to normal tissue because: (a) normal cell viability declines sharply below extracellular pH of 7.1 (Griffith, 1991; Casciari *et al.*, 1992; Stubbs *et al.*, 1994; Gillies *et al.*, 1994; Martin & Jain, 1994), (b) an acidic microenvironment stimulates production of enzymes which degrade the extracellular matrix (Kato *et al.*, 1994; Rozhin *et al.*, 1994), and (c) diminished pH results in loss of intercellular gap junctions reducing the cohesion, collaboration and communication among normal cells at the tumor edge (Yamasaki, 1991). Consequent to this altered microenvironment, progressive loss of normal cells and degeneration of extracellular matrix allows the tumor cells (which are much more resistant to the effects of acidic extracellular pH) to invade the host tissue. Finally, the acid mediation hypothesis of tumor invasion is supported by recent reports (Walenta *et al.*, 2000) that high lactate levels are directly correlated with the likelihood of metastases, tumor recurrence and restricted patient survival.

In modeling the AMTIH, the reaction–diffusion approach is most useful for modeling relatively large (e.g. >0.1 cm diameter), clinically apparent tumors because it describes the "average" behavior of large populations of cells, smoothing out the potentially significant differences in characteristics among the individual cells within the populations. Such models are not effective at describing early tumor growth when only a small number of transformed cells are present. At this stage, tumor growth depends on the discrete history of each individual cell and its interactions with the local environment and adjacent cells.

Thus, to examine the role of H^+ ion production in early tumor growth, it is necessary to develop a mathematical model which includes a discretized approach to describe individual cell interactions while retaining the characteristics of a reaction–diffusion model to describe the microenvironmental changes resulting from H^+ production, diffusion, and removal. We have developed such a model that uses a discrete automaton (Wolfram, 1986; Ermentrout & Edelstein-Keshet, 1993) to describe the cellular interactions and evolution, and differential equations

to model the continuous flow of interstitial H^+ and glucose.

Simple interaction rules between the automaton elements** within the matrix incorporate the effects of the local environment on, and interaction between, tumor and normal cells. The local environment is described by H^+ and glucose concentration fields and their interaction with elements of the matrix are inferred from published experimental work (e.g. glucose uptake, vessel permeability, etc.). The automaton rules allow cells to die, remain quiescent, or divide into adjacent available space over time, depending on the glucose and hydrogen ion concentration in the surrounding environment. Changes in this microenvironment are modeled by the differential equations describing the production, consumption and diffusion of the glucose and hydrogen ions.

In this first paper, in order to keep the space of adjustable parameters manageably small, we have not included all factors of potential influence on tumor growth and invasion. For example, some readers may be surprised that we have not chosen to include oxygen perfusion in this early version of the model. Because of decreased vascularity and blood flow, hypoxia is present in human tumors and is clearly an important factor in certain aspects of tumor biology and treatment. For example, the *in vitro* growth and morphology of multi-cell spheroids is sensitive to diffusion-limited pO_2 (Mueller-Klieser & Sutherland, 1982; Durand, 1983; Sutherland & Durand, 1984). In addition, hypoxia is clearly an important factor in tumor response to radiation as observed both *in vitro* (in multi-cell spheroids, Sutherland & Durand, 1976) and *in vivo* (in metastases of squamous cell carcinomas, Gatenby *et al*., 1988). Because we are concentrating on tumor acidification of the microenvironment, we have chosen not to include oxygen in the current version of our model due to the fact that *in vivo* observations have shown an absence of correlation between hypoxia and reduced interstitial pH within micro-regions of tumor (Helminger *et al*., 1997). This lack of correlation is likely due to two factors: first, tumor glycolytic metabolism is largely independent of local pO_2 so that anaerobic metabolism persists as a major source of cellular energy even in the presence of abundant oxygen (Gullino *et al*., 1967). Therefore, microenvironmental acidification will exist even in normoxic regions of tumor. Second, tumor cell viability in regions far from blood vessels appears entirely independent of oxygen, most likely because glucose diffusivity in tissue is significantly greater than that of O_2 (Vaupel *et al*., 1989). Thus, tumor cells in regions of extreme hypoxia remain viable and metabolically active (resulting in acidification of their microenvironment) because of continued availability of glucose (Mueller-Kleiser *et al*., 1988). Because we are confining ourselves to a study of the effects of microenvironmental acidification on the efficacy of tumor invasion, O_2 perfusion becomes less relevant than other metabolic factors.

O_2 perfusion will become relevant when we include tumor-induced neoangiogenesis. Because there exists evidence that vascular endothelial growth factor (VEGF) may mediate hypoxia-induced angiogenesis (Shweiki *et al*., 1992; Shweiki *et al*., 1995; Liu *et al*., 1999), the next natural step in the evolution of the model is the simultaneous introduction of VEGF production and diffusion, O_2 diffusion, consumption and coupling to VEGF, the destruction of native vascularity and the growth of new vessels. In the absence of these effects the present form of the model is essentially one of pre-neoangiogenic tumor growth, nevertheless, for some combinations of parameters, continued growth and successful invasion (described in detail below) are established by tumor cooption of the native microvessel network. The realization by the model of sustained avascular tumor growth is not an inherent weakness; this growth pattern has in fact been observed in non-small-cell lung carcinoma (Pezzella *et al*., 1997) and in rat C6 gliomas (Holash *et al*., 1999).

We have intentionally chosen this incremental approach to modeling tumor growth and invasion by necessity: the simulations described in this work required over 500 h of computer time on a high performance scientific workstation and, even so, an exhaustive search of parameter space was far from possible. The sole purpose of this

** While "automaton cell" is considered standard terminology, we use "automaton element" when referring to a single member. This is done to avoid confusion with the physical tumor or normal "cells".

paper is to study the *qualitative* relationship between both tumor metabolism and native tissue vascularity on the growth of and invasion efficacy of pre-neoangiogenic tumors.

It is our ultimate goal that the model, as it evolves to include more (and more biologically accurate) first-principles effects, will become useful as a tool to explore diverse hypotheses and to provide insight into the role of various biological parameters in early tumor growth which can then, in turn, guide experimentation and development of new therapies.

Previous Work

Cellular automata have become increasingly important in the modeling of phenomena in many areas of science, especially since Wolfram (1986) demonstrated that every automaton with local interactions belongs to one of a small number of universality classes. This universality of models provides deep insight into analogous behavior of systems as disparate as animal coat patterns and chemical reactions. Biological systems have been particularly amenable to analysis by cellular automata (Ermentrout & Edelstein-Keshet, 1993); so it is not surprising that there is a long history of their use to model tumor growth and other processes important to the development and treatment of cancer. Some of the earliest work in tumor modeling with cellular automata was carried out by Düchting & Vogelsaenger (1984, 1985) to investigate the effects of different radio-therapeutic strategies on tumor growth.

More recently, Qi *et al.* (1993) developed a cellular automaton model of tumor growth in the presence of immune system surveillance and accounting for mechanical pressure from within the tumor. This model is of interest because it recapitulates the Gompertz growth law. The cellular automaton approach was also employed by Smolle & Stettner (1993) and by Smolle (1998a, b) in an attempt to prove relationships between tumor morphology and basic biological features such as cell cohesion, motility and autocrine and paracrine growth factors. Most recently, Kansal *et al.* (2000a, b) have used the Voronoi tessellation of space on which to base a cellular automaton model of brain tumor growth dynamics. This elegant approach allows for the preservation of the discrete nature of cells (or groups of cells) but removes the anisotropy of a regular lattice, from which our model and all those described above suffer.

Neoangiogenesis is another critically important aspect of cancer biology that has been successfully modeled using cellular automata. Chaplain & Anderson (1996) and Anderson & Chaplain (1998) have used cellular automata to solve the discrete version of a system of nonlinear partial differential equations which describe the response in space and time of endothelial cells to tumor angiogenesis factor and fibronectin, including migration, proliferation, anastomosis and branching. The broader topic of vessel morphogenesis has been investigated by Markus *et al.* (1999) using cellular automata to model the development of leaf veins, insect trachea and tumor neovascularization.

In addition to cellular automaton modeling of tumor growth and other processes related to cancer biology and treatment, a wide range of continuum, non-stochastic models of these systems have been successfully developed, primarily using systems of partial differential equations. Just a few of the more recent papers describing such models include: Chaplain & Anderson (1996) (tumor angiogenesis), Adam & Bellomo (1997) (post-surgical response to tumor removal), Olsen *et al.* (1997) (angiogenesis), Ward & King (1997) (avascular tumor growth), Anderson & Chaplain (1998) (tumor angiogenesis), Perumpanani & Norbury (1999) (tumor cell motility during invasion), Sleeman *et al.* (1999) (endothelial motility, chemotaxis and haptotaxis during angiogenesis), Ward & King (1999) (avascular tumor growth saturation) and Jackson & Byrne (2000) (drug resistance and vascular structure in chemotherapy).

To varying degrees, each of the models referred to above, whether automaton-based or continuum, stochastic or deterministic, attempts to capture one, or at most, a few aspects of cancer biology. The model we describe in this paper also focuses on one aspect, namely, the effect of primitive tumor metabolism on the efficacy of tumor invasion. To our knowledge, it is the only model to do so which explicitly includes a random microvascular network from which metabolic substrate is delivered and metabolites removed

through boundary conditions applied at the vessel walls. Other models including diffuse vasculature (e.g., Byrne & Chaplain (1995), for nutrient transfer, and Jackson & Byrne (2000), for chemotherapeutic agent transfer) do so with a spatially uniform term accounting for delivery or removal, not by including individual vessels distributed throughout space. However, as a consistency check against our simulations, and for deriving approximate analytical results for acid production thresholds for tumor invasion, we analyzed a mean-field version of our model with vessels being lumped into a spatially homogeneous term, in much the same manner as Byrne & Chaplain (1995) and Jackson & Byrne (2000). See eqn (16) and its derivation below.

The one work other than our own that addresses the effects of altered tumor metabolism on tumor growth that we are aware of is that of Kraus & Wolf (1996, 1998). These authors have used a discrete approach similar to ours to model tumor growth adjacent to a basement membrane. Our model differs from theirs in that it: (a) employs deterministic dynamics (only our vessel distribution is random), (b) makes no assumption as to the location of the transformed cells with respect to the basement membrane, (c) incorporates microvasculature within the system rather than at the boundaries of the system, and (d) uses glucose diffusion and metabolism as one of the variables.

Methods

A hybrid cellular automaton model is used to simulate early tumor growth. This two-dimensional model is composed of an $N \times N$ array of automaton elements with a specific rule-set governing their evolution as well as hydrogen ion and glucose fields each obeying partial differential equations. The state-vector of each automaton element has four components: (i) the element occupation by either a normal cell, a tumor cell (both in either an active or quiescent state), a micro-vessel or a vacancy resulting from tumor or normal cell death, (ii) the local H^+ ion concentration, (iii) the local glucose concentration, and (iv), in the case of vessels, four ghost values for both chemical fields used to enforce gradient boundary conditions at the four walls of the vessel. *The model enforces a one-to-one correspondence between automaton elements and physical cells comprising the tissue.* Each automaton element, regardless of its state of occupation, has a constant physical size, $\Delta \times \Delta$, where $\Delta = 20$ μm in all of our simulations.

Microvessel automaton elements are randomly distributed throughout the simulation space with density $\phi_v = N_v/N^2$, where N_v is the number of automaton elements occupied by a microvessel. In the physiology literature, microvessel density is usually expressed as an *areal* density, α, i.e., the surface area of vessels per unit volume, so that in the limit of small ϕ_v we have the relationship $\alpha = 4\phi_v/\Delta$. No restriction is imposed upon how many automaton elements are allowed to cluster together to form a vessel. While the overall positioning of the microvessels is random, there are short-range correlations induced by the requirement that any individual tumor or normal cell has only a single vessel as a nearest neighbor, otherwise the value of the chemical fields within cells with two or more neighboring vessels would be over-determined by the multiple boundary conditions imposed (see eqns (4) and (7) and the discussion leading to eqn (12)). Essentially, this condition requires that any cluster of automaton elements forming a vessel have a convex perimeter, fortunately a property of real blood vessels.

The H^+ and glucose concentrations form two continuous fields over the simulation space (i.e., all automaton elements) obeying suitable time-dependent diffusion equations with sinks, sources, and boundary conditions determined by the distribution of cells and vessels. The simulation begins with the establishment of either a 100×100 or 200×200 matrix of automaton elements occupied by normal tissue and a random distribution of vessels at density ϕ_v. The resulting glucose profile is determined and a uniform pH of 7.4 is established. A starting population of tumor cells in a disk shape with a diameter of five cells (total of 21 cells) is then introduced at the center of the system replacing any normal cells or vessels originally occupying these automaton elements. The temporal evolution of the competing populations is then observed. The time-scale for temporal development of the automaton elements is determined by the application of the rules described below for the passing of each cellular generation.

AUTOMATON RULES

The rules governing the evolution of the automaton elements are quite straightforward:

(a) If the occupancy of an automaton element is either micro-vessel or vacant it does not evolve directly, although in the latter case it can evolve indirectly by the division of a tumor or normal cell occupying an adjacent element.

(b) If the occupancy of an automaton element is either tumor or normal then the H^+ ion and glucose concentration component of its state-vector are considered. If the local $pH = -\log(H^+)$ is less than a critical threshold for the normal or the tumor cells, namely, pH_N^D and pH_T^D, then the cell will die and the element's state will be changed to "vacant". In all of the simulations described herein, these thresholds were taken to be $pH_N^D = 6.8$ and $pH_T^D = 6.0$ (Dairkee *et al.*, 1995). If the local pH is greater than pH_N^D (pH_T^D) but less than a second threshold, pH_N^Q (pH_T^Q), then the normal (tumor) cell survives in a *quiescent* state (i.e., mitosis does not occur). These quiescence thresholds were taken to be $pH_N^Q = 7.1$ and $pH_T^Q = 6.4$ for normal cells and tumor cells, respectively (Casciari *et al.*, 1992). Some preliminary simulations were performed with $pH_T^Q \leqslant 6.4$.

(c) If the cell survives because the local pH is above its threshold value then it will be given the opportunity to divide provided that there is adequate substrate and local $pH > pH_N^Q$ for normal cells or $pH > pH_T^Q$ for tumor cells. The glucose levels above which a cell can survive, G_N^D and G_T^D for normal and tumor cells, respectively, were each taken to be 2.5 mM (the serum level below which serious hypoglycemic effects manifest themselves; see, for example, Ganong, 1999) in all of the simulations described herein. Furthermore, a cell is only allowed to divide if there are one or more neighboring elements that are vacant. In the case of multiple vacant neighbors, the one with the highest glucose level will receive the daughter cell and its state will be updated accordingly.

After the automaton element occupancies have been updated, the remaining components of their state-vectors must reflect these changes. To do so, the evolution of the chemical fields is determined by solving two differential equations.

SOLUTION OF THE BOUNDARY-VALUE PROBLEMS

A large disparity exists between the time-scales of cell proliferation and chemical diffusion. The cell doubling time is of order 10^2 h (Marušic *et al.*, 1994; Rew & Wilson, 2000) whereas the inter-vessel diffusion time for lactic acid and glucose is only of order 1–10 s (e.g., with mean intervessel distance $\Delta x = 10^{-2}$ cm and lactic acid diffusion constant $D_H = 1.08 \times 10^{-5}$ cm^2/s the diffusion time is given by $\Delta\tau = (\Delta x)^2/D_G = 9.3$ s). This affords a useful approximation for the temporal development of the substrate and by-product fields: cellular distributions change so slowly on the time-scale of chemical diffusion that these changes can be treated as *adiabatic perturbations* on the chemical fields. Therefore, the evolution of the chemical fields need not be found by solving parabolic diffusion equations explicitly in time, but rather by *solving a sequence of equilibrium, elliptic boundary-value equations on a much coarser time-scale*. While this approximation greatly improves simulation efficiency, it does introduce spurious correlation in the system because all cells within a characteristic diffusion length respond to changes in the chemical fields simultaneously. To remove these correlations we advance the automaton in a series of *sub-generations* by first choosing a random sub-set of automaton elements for updating, that is, only a certain fraction, $f < 1.0$, of automaton elements are updated according to the above rules during each sub-generation. We then solve the equilibrium boundary value problems to determine the resultant response of the chemical fields. This process is repeated $1/f$ times until all automaton cells have been updated, i.e., one *generation* of the automaton has passed. Through a series of tests, we have found no qualitative difference in the evolution of the automaton provided that $f < 0.2$; therefore, in all of the simulations described herein we have taken $f = 0.1$, i.e., ten sub-generations.

The full diffusion equation describing the time-dependent glucose field, $G(\mathbf{r}, t)$ is

$$D_G \nabla^2 G(\mathbf{r}, t) - k(\mathbf{r}) G(\mathbf{r}, t) = \frac{\partial G(\mathbf{r}, t)}{\partial t}, \qquad (1)$$

where $\mathbf{r}$ is the position vector in the simulation space, t is time and $D_G = 9.1 \times 10^{-5}$ cm^2/s is the

glucose diffusion constant (Crone & Levitt, 1984). Using the adiabatic perturbation approximation described above, eqn (1) becomes

$$D_G \nabla^2 G_t(\mathbf{r}) - k(\mathbf{r}) G_t(\mathbf{r}) = 0, \tag{2}$$

where $G_t(\mathbf{r})$ is the glucose concentration at $\mathbf{r}$ after sub-generation t. The term $k(\mathbf{r})$ (having units $1/s$) in eqns (1) and (2) is the glucose consumption rate at the location $\mathbf{r}$:

$$k(\mathbf{r}) = \begin{cases} k_N & \forall \mathbf{r} = \text{Normal Cells}, \\ k_T & \forall \mathbf{r} = \text{Tumor Cells}, \\ 0 & \forall \mathbf{r} = \text{Vacant Cells}, \\ 0 & \forall \mathbf{r} = \text{Vessel Cells}, \end{cases} \tag{3}$$

where $1 \times 10^{-6}/\text{s} < k_N < 5 \times 10^{-4}/\text{s}$ and $1 \times 10^{-5}/\text{s} < k_T < 1 \times 10^{-3}/\text{s}$ are ranges for glucose consumption by normal and tumor cells, respectively (Kallinowski *et al.*, 1988; Kallinowski & Vaupel, 1988; Casciari *et al.*, 1992; De Gaetano & Arino, 2000). In all simulations herein we have set $k_N = 1 \times 10^{-4}/\text{s}$ and $k_T = 1 \times 10^{-3}/\text{s}$.

Glucose enters the system through boundary conditions at the vessel walls enforcing that the flux (i.e. $\mathbf{J} = -D_G \nabla G$) through the vessel wall be proportional to the concentration difference across it, the constant of proportionality being the vessel permeability q_G. Thus,

$$-\mathrm{D}_G \hat{n} \cdot \nabla G_t|_{wall} = q_G (G_S - G_t|_{wall}), \tag{4}$$

where $\hat{n}$ is the unit normal vector pointing orthogonally outward from the vessel wall and G_S is the serum glucose level. We take the permeability to be $q_G = 3.0 \times 10^{-5}$ cm/s (Crone & Levitt, 1984) and serum glucose to be $G_S = 5.0$ mM (Kratz & Lewandrowski, 1998) in all of our simulations.

The acid profile is found in much the same way; however, the boundary-value equation is slightly different:

$$D_H \nabla^2 H_t(\mathbf{r}) + h(\mathbf{r}) = 0, \tag{5}$$

where $D_H = 1.08 \times 10^{-5}$ cm^2/s (Crone & Levitt, 1984) is the diffusion constant for lactic acid, $H_t(\mathbf{r})$ is the H^+ concentration at position $\mathbf{r}$ after sub-generation t, and $h(\mathbf{r})$ is an acid production rate that is non-zero only at positions $\mathbf{r}$ where there is a tumor cell:

$$h(\mathbf{r}) = \begin{cases} \dot{H}_T^A & \forall \mathbf{r} = \text{Active tumor cells}, \\ \dot{H}_T^Q & \forall \mathbf{r} = \text{Quiescent tumor cells}, \\ 0 & \forall \mathbf{r} \neq \text{Tumor cells}. \end{cases} \tag{6}$$

In our model, $\dot{H}_T^A$ and $\dot{H}_T^Q$ are key variables adjusted to model tumor phenotypes expressing different metabolisms: $1 \times 10^{-5} < \dot{H}_T^A < 1 \times 10^{-4}$ mM/s and $\dot{H}_T^Q = 5 \times 10^{-7}$ mM/s.†† Solutions of eqn (5) must satisfy boundary conditions at the vessel walls analogous to eqn (4) for glucose, namely,

$$-D_H \hat{n} \cdot \nabla H_t|_{wall} = q_H (H_S - H_t|_{wall}), \tag{7}$$

where $q_H = 1.19 \times 10^{-4}$ cm/s is the vessel permeability to lactic acid (Crone & Levitt, 1984) and $H_S = 3.98 \times 10^{-5}$ mM is the serum acid concentration, i.e. pH = 7.4. This boundary condition and the one in eqn (4) were applied only at vessel walls; periodic boundary conditions on both $G(\mathbf{r})$ and $H(\mathbf{r})$ were enforced at the automaton perimeter as well. Tumor glucose consumption and acid production were intentionally decoupled to provide maximum flexibility in exploring the parameter space by simulation.

Computer simulations of a 100×100 matrix of automaton elements (200×200 for selected parameters) were performed for 40 generations using the *C* programming language running on a DEC Alpha UNIX workstation. Simulations were performed over a range of vascular densities, ϕ_v, and a range of H^+ production by active tumor cells, $\dot{H}_T^A$, while keeping all other parameters constant. For a given $\phi_v - \dot{H}_T^A$ pair, results were averaged over at least ten repetitions of the evolution of the system (20 or more repetitions in regions of

†† This range of values for $\dot{H}_T^A$ is somewhat less than actual tumor acid production rates (e.g. those determined from data reported by Kallinowski & Vaupel, 1988; Casciari *et al.*, 1992) and was used because our model does not explicitly include chemical buffering but only allows for acid removal through vessels. However, the range chosen accurately produces extracellular pH observed in tumors *in vivo*. The value of of $\dot{H}_T^Q = \dot{H}_T^A/100$ was chosen to model quiescent tumor cells, as they are essentially metabolically inactive.

parameter space where fluctuations were large), each differing only in the random distribution of vessels.

Eqns (2) and (5) were numerically solved by the method of simultaneous over-relaxation with Chebyshev acceleration (Press *et al.*, 1996). This method proceeds by first writing the differential equation in terms of finite-differences, e.g., eqn (2) would become:

$$\frac{G_{i+1,j} + G_{i-1,j} + G_{i,j+1} + G_{i,j-1} - 4G_{i,j}}{\Delta^2} - \frac{k_{i,j}}{D_G} G_{i,j} = 0, \tag{8}$$

where the first term in eqn (8) is the centered-difference approximation to the two-dimensional rectangular Laplacian operator acting on G. The subscripts i and j are the row and column indices of the automaton elements, thus $k_{i,j}$ refers to the glucose consumption rate of the i–jth automaton element which depends on its occupancy [see eqn (3)]. Equation (8) can be written as $\forall i \in (1, N)$ and $\forall j \in (1, N)$, and is thus representative of a system of N^2 linear algebraic equations in the unknown $G_{i,j}$, where the automaton matrix of elements is of size $N \times N$.

Equation (8) can be rearranged and its *residual* $\xi_{i,j}$ defined to be

$$\xi_{i,j} = G_{i+1,j} + G_{i-1,j} + G_{i,j+1} + G_{i,j-1} - \left(4 + \frac{\Delta^2 k_{i,j}}{D_G}\right) G_{i,j}. \tag{9}$$

Successive over-relaxation is an iterative procedure whereby an approximate solution of (8), $G_{i,j}^{Old}$, is improved by iterating

$$G_{i,j}^{New} = G_{i,j}^{Old} + \omega \frac{\xi_{i,j}^{Old}}{4 + (\Delta^2 k_{i,j}/D_G)}, \tag{10}$$

where $1 < \omega < 2$ is a *relaxation parameter* optimally chosen to reduce the norm of $\xi_{i,j}$ to an arbitrarily small value (Press *et al.*, 1996) as the iteration proceeds. Iteration begins at some physically reasonable guess such as $G_{i,j}^{Guess} = G_S \; \forall i, j$, where G_S is the serum glucose level.

The only complication to this procedure is when the i–jth element in eqn (8) is adjacent to an element occupied by a vessel. In this case, the boundary condition in eqn (4) must be applied. For concreteness, assume the vessel is at element $(i, j-1)$, then $G_{i,j-1}$, being within a vessel, is *outside* of the system. It is incorrect to simply make the substitution $G_{i,j-1} = G_S$ into eqn (8) and continue with the rest of the solution because eqn (4) will not be satisfied at the vessel wall, that is at (i, j) (or for that matter at the walls of the remaining three nearest-neighbors of $(i, j-1)$). The correct approach is to write (4) as

$$-D_G \frac{G_{i,j} - G_{i,j-1}}{\Delta} = q_G(G_S - G_{i,j}), \tag{11}$$

where the directional-derivative has been approximated with a forward finite-difference: $\hat{n} \cdot \nabla G|_{i,j} \approx (G_{i,j} - G_{i,j-1})/\Delta$. Equation (11) is then solved for $G_{i,j-1}$ giving

$$G_{i,j-1} = G_{i,j} + \frac{q_G \Delta}{D_G}(G_S - G_{i,j}). \tag{12}$$

When eqn (12) is substituted into eqn (8) it becomes

$$G_{i+1,j} + G_{i-1,j} + G_{i,j+1} - \left(3 + \frac{\Delta^2 k_{i,j} - q_G \Delta}{D_G}\right) G_{i,j} = \frac{q_G \Delta}{D_G} G_S. \tag{13}$$

Thus, the only effect of the boundary conditions at the vessel walls is to change the coefficients of the G's in the linear equations for the adjacent elements. An identical method is used for applying the boundary condition (7) when solving eqn (5). To validate our algorithm for solving the boundary-value equations, we compared our numerical solutions with exact Fourier series solutions for a regular pattern (square lattice) of vessels and with solutions generated by *Matlab* for a random vessel distribution. In both cases, the agreement was excellent.

For the purpose of analysis, we characterized tumor size by the radius of gyration of the entire tumor including regions of tumor necrosis but

not normal tissue necrosis. The radius of gyration is defined to be the square root of the second moment of this spatial distribution. This quantity was recorded for each generation of the automaton and when a particular simulation was completed, typically after 40 generations, the data were analysed using linear regression over the last ten generations.‡‡ Using the slopes of these regression lines, the tumor growth rate and its statistical uncertainty were recorded for each simulation.

The most trivial model of (two-dimensional) tumor growth assumes that the time rate of change of the tumor area is proportional to its perimeter, thus predicting that the tumor radius should grow linearly with time. Interestingly, even with the inclusion of blood vessels, competition for space and resources, and all of the other complexities of the model described above, this was still found to be true for a wide range of parameters. In certain extreme cases, either early-time transients or late-time deviations from a constant growth rate were observed.

In our cellular automaton model, both the tumor and normal cells are given the opportunity to divide once per generation. However, it is well known that the mitotic rate for transformed cells is generally higher than that for cells found in normal tissue. For the range of parameters studied, this discrepancy does not introduce any artifacts in the cell growth dynamics. This is because normal tissue recovery is never sufficiently robust to impede the advancing tumor by competing for space within a "hypocellular gap" which forms at the tumor–host interface (see the discussion below). Thus, even though our normal cells have the potential to divide at an unrealistically high rate, they are always at a disadvantage with respect to the tumor cells in the adverse microenvironment of the acidic hypocellular gap. Therefore, the result is a lower net mitosis rate for normal cells.

‡‡ For all of the cases studied herein this was a sufficiently late time to avoid initial transients but not so late as to be affected by the finite-size of the system. Even for cases where the late time growth rate was not constant, a straight-line approximation over the short span of the last ten generations gave a reasonable estimate of the growth rate.

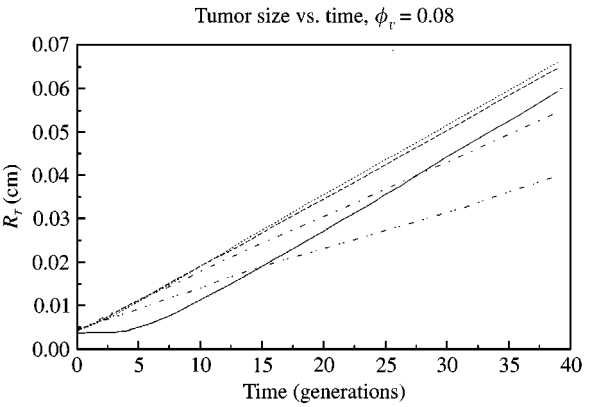

FIG. 1. Tumor radius of gyration is plotted as a function of time for a sequence of increasing acid production rates but with vessel density held fixed. Note the monotonic decrease in the late-time slope (growth rate) as $\dot{H}_T^A$ increases. This correlation is reversed if the vessel density is sufficiently high (c.f. Fig. 4). Also, note the early-time, nonlinear transient period for the lowest acid production case ($\dot{H}_T^A = 2.5 \times 10^{-5}$ mM/s) wherein initial tumor growth is postponed until adequately high H^+ concentration has accumulated. (——) $\dot{H}_T^A = 2.50 \times 10^{-5}$ mM/s; (·····) $\dot{H}_T^A = 2.75 \times 10^{-5}$ mM/s; (------) $\dot{H}_T^A = 3.00 \times 10^{-5}$ mM/s; (- · - ·) $\dot{H}_T^A = 5.00 \times 10^{-5}$ mM/s; (– ··) $\dot{H}_T^A = 8.00 \times 10^{-5}$ mM/s.

Results

The simulations involved systematically varying vascular density, ϕ_v, and H^+ production by active tumor cells, $\dot{H}_T^A$, while keeping other parameters constant. Multiple repetitions of the evolution of the system for each $\phi_v - \dot{H}_T^A$ pair (differing only in the random distribution of vessels) were performed to obtain adequate statistics. Additional single computer runs with parameters other than ϕ_v and $\dot{H}_T^A$ being varied were performed as needed.

In Fig. 1, the temporal evolution of the tumor radius of gyration, R_T, is plotted against time measured in automaton generations. For simplicity, we show the evolution of the system for only one value of vascular density ($\phi_v = 0.08$), however, results for five different tumor phenotypes (differing only in their degree of tumor acid production) are presented. With the exception of the case with the least tumor acid production ($\dot{H}_T^A = 2.5 \times 10^{-5}$ mM/s), tumor growth is linear from the earliest time. In every case shown, the late-time growth rate is essentially constant and is observed to decrease with increasing acid production. While this correlation between growth rate and acid production may seem contradictory

to the acid mediation hypothesis for tumor invasion, it must be remembered that host tissue vascularity is a parameter of critical importance to the dynamics of tumor growth. As will be discussed below, this correlation is completely *reversed* for sufficiently high ϕ_v. The importance of the relationship between this reversal and the effects of neoangiogenesis on tumor growth are obvious.

In Fig. 2 the temporal evolution of a typical ($\phi_v = 0.08$, $\dot{H}_T^A = 3.0 \times 10^{-5}$ mM/s) tumor is shown on a 200×200 matrix of automaton elements. By the fifth generation a well-defined hypocellular gap (black) has formed before the tumor front, thus facilitating its advance. This hypocellular region was also observed in simulations of the reaction-diffusion model of the AMTIH and approximate analytical estimates of its width as a function of basic parameters were made [see Gawlinski & Gatenby (1996), in which evidence for the existence of this hypocellular zone based on *in vitro* experiments and pathologic specimens is presented]. Note that a ring of quiescent normal cells (dark blue) surrounds the gap. The interface between these two regions is where the acid concentration has dropped from its maximum (deep within the tumor) to a point such that local $\mathrm{pH} = \mathrm{pH}_H^D = 6.8$. The interface between the quiescent normal cells and the active normal cells (bright blue) is where the acid concentration has further dropped to the point where local $\mathrm{pH} = \mathrm{pH}_N^Q = 7.1$. By the tenth generation the tumor comprises a ring of active tumor cells (bright red) surrounding a core of diffusely mixed active and quiescent tumor cells (dark red). Lastly, note that, for late time, as the tumor grows the widths of the three concentric rings of quiescent normal, necrotic, and active tumor remain approximately constant, and that the composition of the tumor core (i.e. the ratio of active to quiescent tumor cells) is unchanging. This observation indicates that the acid profile of the tumor front is propagating as an invariant traveling wave in much the same way as found by Gatenby & Gawlinski (1996) using reaction-diffusion equations.

Quite different tumor morphologies and dynamics than those depicted in Fig. 2 can emerge depending on tumor metabolism and native vascularity. In Fig. 3 we present four different tumors that have been growing for the same amount of time (40 generations), each starting from the same size. In Fig. 3a and b both the vessel fraction and the acid production rate are taken relatively high ($\phi_v = 0.18$ and $\dot{H}_T^A = 1.8 \times 10^{-4}$ mM/s), however in Fig. 3a tumor quiescence is admitted by setting $\mathrm{pH}_T^Q = 6.4$ and in Fig. 3b it is suppressed by setting $\mathrm{pH}_T^Q = 6.0$ (recall that $\mathrm{pH}_T^D = 6.0$ in all simulations). Morphologically the end results are similar, with the exception that necrotic sites in Fig. 3b have replaced the diffuse quiescent tumor sites observed in Fig. 3a. However, the dynamics are strikingly different, with the necrotic tumor growing at a rate 50% greater than the solid tumor with quiescent regions. This is an example of growth enhancement at the expense of the tumor itself (diffuse necrosis), a behavior seen only in situations of high vascularity. Presumably, such growth enhancements could be sustained as well by a high non-native vascularity provided by tumor-initiated neoangiogenic activity.

Lowering both the vascularity (to $\phi_v = 0.08$) and the acid production rate (to $\dot{H}_T^A = 3.0 \times 10^{-5}$ mM/s) while keeping tumor quiescence suppressed ($\mathrm{pH}_T^Q = 6.0$) results in the formation of a compact tumor with regions of central necrosis (Fig. 3c). However, if the vascularity is lowered further to $\phi_v = 0.04$ the tumor initially grows but soon "self poisons", surviving only in cords around blood vessels (Fig. 3d). The tumors depicted in Fig. 3a–c have constant late-time growth rates, whereas that in Fig. 3d does not; its growth rate is decreasing with time. Once again, if the tumor depicted in Fig. 3d were to acquire additional blood supply through neoangiogenesis it would resume aggressive growth.

The growth pattern observed in Fig. 3d are quite similar to those observed *in vivo* by Holash *et al.* (1999) where pre-neoangiogenic growth and invasion is accomplished by the tumor's cooption of the host's existing microvessel network. Holash *et al.* characterize the clumps of tumor cells adhering to native vessels as "cuffs".

In Fig. 4, the tumor growth rate, $\dot{R}_T$, is plotted against the vascular density, ϕ_v, for five different values of $\dot{H}_T^A$. This set of plots shows that for a given $\dot{H}_T^A$, there is a range of vascular density for which tumor growth is optimal. For high

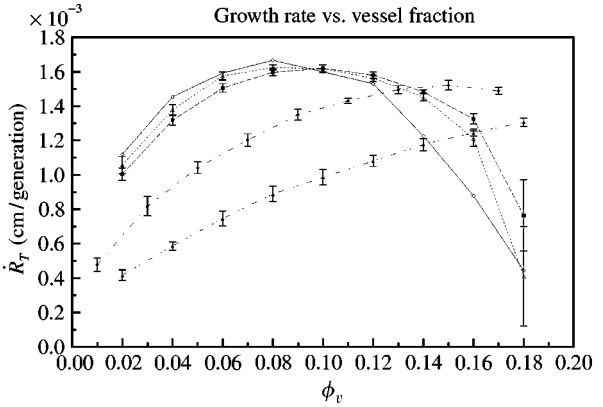

FIG. 4. Growth rates measured in centimeters of radius of gyration increase per generation are plotted versus vascular density for a sequence of acid production rates. With the exception of the highest acid production rate, each curve has a maximum associated with the optimal tradeoff between auto-toxicity and the efficient removal of acid by the native vascular network (presumably, even the $\dot{H}_T^A = 8.0 \times 10^{-5}$ mM/s case would reach a maximum, albeit at a large, physiologically unrealistic ϕ_v). Note that for low ϕ_v the growth rate decreases with increasing $\dot{H}_T^A$, but for high ϕ_v this trend is reversed (again, excluding the $\dot{H}_T^A = 8.0 \times 10^{-5}$ mM/s, case with maximum off the graph). Data points are mean values averaged over 20 different random vessel distributions; error bars represent the standard error of the mean. (◇ ——) $\dot{H}_T^A = 2.50 \times 10^{-5}$ mM/s; (△ ·····) $\dot{H}_T^A = 2.75 \times 10^{-5}$ mM/s; (■ – – –) $\dot{H}_T^A = 3.00 \times 10^{-5}$ mM/s; (◆ – ·) $\dot{H}_T^A = 5.00 \times 10^{-5}$ mM/s; (▲ – ··) $\dot{H}_T^A = 8.00 \times 10^{-5}$ mM/s.

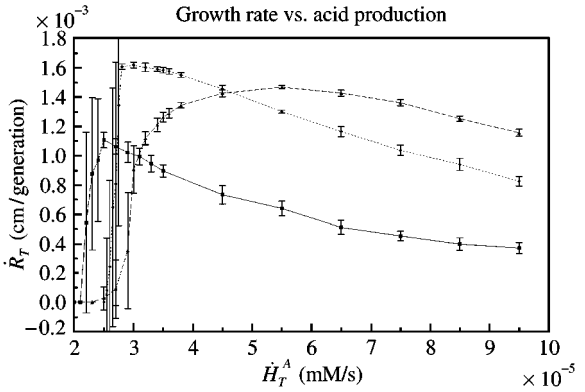

FIG. 5. Growth rates measured in centimeters of radius of gyration increase per generation are plotted versus acid production rate for a sequence of vessel densities. In each case, when the acid production rate is very low the initial tumor seed is essentially confined, however as $\dot{H}_T^A$ is increased through a narrow transition zone, tumor growth rapidly commences. The position of this transition increases with ϕ_v and can be fairly well predicted by a mean-field argument [see text leading to eqn (16)]. The monotonic decrease in growth rate at large values of $\dot{H}_T^A$ is a result of auto-toxicity. (■ – – –) $\phi_v = 0.02$; (◆ – ·) $\phi_v = 0.10$; (▲ – ··) $\phi_v = 0.18$.

vascularity ($\phi_v > 0.16$) and low acid production ($\dot{H}_T^A < 3.0 \times 10^{-5}$ mM), the growth rate is very low, however as the vascularity is lowered, the growth rate increases, reaching a maximum somewhere in the range of $0.08 < \phi_v < 0.10$. To our knowledge, this correlation has not been explicitly tested or observed in the literature. It is consistent, however, with clinical observation that tumors grow in disordered tissue with altered vascularity (e.g. hepatocellular carcinoma in cirrhotic livers, lung cancer in chronically inflamed bronchi, and colon cancer in adenamatous polyps). Further reduction of ϕ_v from the 0.08–0.10 range results in diminished aggressiveness due to an accumulation of acid to a degree unfavorable to the tumor itself. Presumably, these correlations hold for high acid production rates as well ($\dot{H}_T^A > 5.0 \times 10^{-5}$ mM), however unrealistically high vascular densities would be required to confer protection against invasion by these aggressive phenotypes.

Fig. 5 shows the relationship between the growth rate, $\dot{R}_T$, and the acid production rate, $\dot{H}_T^A$, for three values of ϕ_v. Two important features are apparent in this figure: First, increasing $\dot{H}_T^A$ beyond 5×10^{-5} mM results in a monotonic decrease in growth resulting from the tumor auto-toxicity mentioned above, with the effect being more dramatic with decreasing vessel density. Second, there appears a sharp transition from a slow or zero growth regime to one of rapid growth as $\dot{H}_T^A$ is increased through a threshold that increases with vessel density. This same sharp transition from a benign to frankly malignant state has also been observed in the reaction-diffusion model of the AMTIH where it has been identified as a bifurcation in the underlying dynamical system and shares a similarity with the adenoma–carcinoma sequence (Gatenby & Gawlinski, 1996). The effect of the basic biological parameters critical to controlling this bifurcation is supported by experiment and clinical observation.

Estimates of the locations of these transitions as a function of ϕ_v (and other system parameters) can be extracted from a mean-field version of the model in which the randomly positioned vessels

are replaced by a spatially homogenous acid uptake term chosen such that it is capable of removing an amount of acid equivalent to the discrete vessels. Thus, for a tumor of radius r_0, equation (5) becomes in the mean-field approximation:

$$D_H \nabla^2 H(r) + \dot{H}_T^A = 0, \qquad r \leqslant r_0,$$

$$D_H \nabla^2 H(r) + \frac{4\phi_v q_H}{\Delta} [H_S - H(r)] = 0, \quad r > r_0. \tag{14}$$

There is no acid uptake term in eqn (14) for $r < r_0 \approx 50$ μm because our initial tumor seed is avascular. The solution of eqn (14) at the tumor boundary $r = r_0$ is:

$$H(r_0) = H_S + \frac{k_2 r_0 K_0(\sqrt{k_1} r_0)}{2\sqrt{k_1} K_1(\sqrt{k_1} r_0)}, \tag{15}$$

where $k_1 = 4\phi_v q_H / \Delta D_H$, $k_2 = \dot{H}_T^A / D_H$ and $K_{0,1}$ are modified Bessel functions. The tumor will only grow if $H(r_0) > H_D^N$, where $H_D^N = 1.58 \times 10^{-4}$ mM ($\mathrm{pH}_D^N = 6.8$) is the acid threshold for normal cell death. Equation (15) can be inverted to obtain an estimate of the acid production threshold, $\dot{H}_T^{A^*}$, for the onset of growth

$$\dot{H}_T^{A^*} \geqslant \frac{2D\sqrt{k_1} K_1(\sqrt{k_1} r_0)(H_N^D - H_S)}{r_0 K_0(\sqrt{k_1} r_0)}. \tag{16}$$

Equation (16) predicts threshold values of $\dot{H}_T^{A^*} = 2.2 \times 10^{-5}$, 3.0×10^{-5} and 3.9×10^{-5} mM/s for $\phi_v = 0.02$, 0.10, and 0.18, respectively, in reasonably good agreement with the thresholds observed in Fig. 5.

While the solution of eqn (2) at each generation resulted in significant glucose gradients (G varying between 3.0 mM deep within compact tumors to 4.3 mM in normal tissue with vessel fraction $\phi_v = 0.04$), no intercellular glucose levels approaching the cell death threshold ($G_N^D = G_T^D = 2.5$ mM) were observed. This result of a system fairly well perfused by substrate indicates that local competition for resources between tumor and host is most likely not a mechanism for tumor invasion, at least for the glucose-related parameters studied herein. However, if there exist tumor phenotypes with substantially higher substrate requirements then competition for resources could become a significant factor.

Discussion

We have developed a hybrid cellular automaton model of early tumor growth that describes the activity of individual cells and the continuous evolution of their microenvironment. Clinically apparent tumors are well characterized by mathematical models employing only differential equations because the large number of cells present allows averaging of the behavior of a population without significant loss of accuracy. This approach is not readily applicable to early tumor growth when only a small number of tumor cells are present. During this stage of tumorigenesis, the discrete history of each individual cell and its interactions with the microenvironment and adjacent cells must be examined. The approach presented here employs a cellular automaton matrix to describe the cell–cell interactions, while simultaneously modeling the continuous processes in the microenvironment with differential equations governing superimposed chemical fields.

This mathematical model was developed primarily to study the roles of H^+ production and native vascularity in early tumorigenesis (prior to neoangiogenesis). Previously published models of invasive growth in clinically apparent tumors have suggested that tumor-induced acidification of the microenvironment was critical for invasion and destruction of adjacent normal tissue (Gatenby, 1991, 1995; Gatenby & Gawlinski, 1996). It was not clear, however, that the acid production by tumor cells in very early tumorigenesis, when only a very small number of tumor cells exist, would be sufficient to significantly alter the microenvironment. The hybrid cellular automaton approach allows extension of this hypothesis to early tumor growth that has not previously been modeled. In general, our simulations demonstrate that a small clone of tumor cells will develop into a clinically important malignancy if the clonal phenotype alters the local microenvironment so that it is hostile to

normal cells but favorable to growth of cells in the clone. This appears to depend on the balance between the amount of acid the tumor clone produces and the amount that is buffered or removed by the local blood flow. Specific insights concerning early tumor growth derived from this model include the following:

First, within the context of the model, excess H^+ production by even a small number of tumor cells is sufficient to alter the microenvironment and promote invasive tumor growth. In general, for an optimal range of microvessel density (ϕ_v), as the H^+ produced per unit time ($\dot{H}_T^A$) increases, the tumor becomes more aggressive and invasive. If H^+ production falls below some critical value, tumor growth rate is dramatically reduced, in some instances to zero (see Fig. 5). In addition, for any given degree of vascularity, if H^+ produced is sufficiently high, the microenvironment becomes too acidic for any cell survival (tumor or normal) and the tumor essentially becomes auto-toxic.

Second, the model explicitly examines the role of vascularity in different stages of early tumor growth. Essentially, for any given rate of acid production the model predicts a range of optimal vascular density (see Fig. 4). Thus, increased vascular density (above the optimal range) is seen to decrease the growth of a small tumor clone because it facilitates buffering and elimination of the excessive H^+, maintaining a microenvironment favorable to normal tissue in its competition for space with the transformed cells.§§ The clinical significance of this result is not clear, particularly because the required vascular density for observing the effects may be greater than that typically found under physiological conditions (e.g. see the curves for $\dot{H}_T^A = 5.0 \times 10^{-5}$ and 8.0×10^{-5} mM/s in Fig. 4). Nevertheless, the model does suggest that tumor growth in highly vascularized normal tissue may be impeded (note that the model predicts only a slowing of the growth rate under these conditions, not a cessation or reversal of growth). We know of no studies that have explicitly tested the model prediction but speculate that this mechanism may play a role in the limited growth of metastases observed in the kidney and spleen. Autopsy studies have shown that small metastases are very common in these highly vascularized organs (incidence of 8–13% in the kidneys in autopsy series of patients with metastatic carcinoma (Abrams *et al*., 1950; Klinger, 1951; Newsam & Tullock, 1966; Wagle *et al*., 1975)) but are rarely apparent clinically because they fail to grow to sufficient size to produce symptoms. However, there are so many other uncontrollable variables *in vivo* that, at best, we can say such observations are consistent with the hypothesis, but certainly do not provide definitive proof. On the other hand, if this mechanism is indeed clinically relevant, there is a possibility that a reduction in vascularity (e.g. by the therapeutic administration of anti-angiogenesis factors) will actually result in an environment more favorable to the growth of some small tumor clones, and therefore a paradoxical increase in clinically apparent metastatic disease.

A vascular density below the optimal range is also seen to inhibit tumor growth because it results in acid accumulation and tumor auto-toxicity as described above. Although angiogenesis is not part of the current model, it is reasonable to conclude that the latter, in general, supports the notion that for a specific $\dot{H}_T^A$, especially with ϕ_v in the auto-toxic domain, increasing vascularity will aid in tumor growth. This supports the increasingly popular concept of treating tumors with agents that inhibit angiogenesis (Folkman, 1989; Folkman *et al*., 1992; Shant *et al*., 1999). However, the model adds the caveat that even significant decreases in tumor vascular density may not result in tumor regression if the density remains in the broad range favorable to tumor growth.

A limitation of the current simulation is that the evolution of the vascular network, either through low pH-induced disruption or through neo-angiogenesis, has not been studied. However, it is reasonable to extrapolate that, depending on the tumor phenotype and the remaining local vascularity, a more favorable or detrimental environment may be created for the tumor. For example, in the case of high acid production,

§§ Contrast this effect with the advantage acquired through tumor induced angiogenesis, specifically better O_2 and substrate perfusion and acid removal. We intend to explore the relative importance of these two competing effects by simulation of an extended automaton model.

it is expected that including native vessel disruption results in the curve in Fig. 4 shifting to the right (auto-toxicity enhanced); including neo-angiogenesis causes a shift to the left (auto-toxicity diminished). For other combinations of $\phi_v - \dot{H}_T^A$ pairs, the effects are more difficult to predict and must await further simulation of a more detailed model.

Support for the accuracy of the mathematical model arises from its ability to reproduce many of the known characteristics of tumor morphology. Specific combinations of tumor H^+ production and vascularity are shown to result in varying patterns of tumor growth similar to those observed microscopically in human malignancies including tumor cords, central necrosis, diffuse necrosis and tumor edges which can be "pushing"‖‖ or "invasive". In addition, a hypocellular gap at the tumor host interface is reproduced as first predicted by Gatenby & Gawlinski (1996).

Finally, the model poses new interesting questions with therapeutic implications. This largely stems from the observations that both too little and too much interstitial H^+ can thwart tumor growth. Can the former be accomplished, by reduction in tumor H^+ production through reduction of glucose uptake (hence increasing the pH) or reduction in H^+ excretion (decreasing the intracellular pH and increasing the extracellular pH) through inhibition of the Na^+/H^+ antiporter system? One study, for example, has demonstrated significant reduction in the development of metastases by amiloride (Tannock & Rotin, 1989). Increased H^+ levels can be accomplished by reduction in tumor vascularity consistent with anti-angiogenesis therapies or by increasing Na^+/H^+ antiporter activity. Could either reduction of extracellular pH below the optimal level by the above method or systemic acidification have therapeutic implications? This strategy is consistent with some animal model observations noting an antitumor effect from systemic acidification (Harguindey *et al.*, 1979). We also pose a question: could the well-documented phenomenon of regression of metastases from renal carcinoma following resection of the primary (Yoshino & Wakui, 1988; Koike *et al.*, 1990; De Riese *et al.*, 1991; Garcia Tabar *et al.*, 1992) actually be the result of systemic acidification following nephrectomy? Obviously, these questions need to be further studied both clinically and experimentally before making statements about therapeutic implications in humans.

Our hybrid cellular automaton model described herein is a significant improvement over our fully deterministic reaction–diffusion model of the AMTIH (Gatenby & Gawlinski, 1996). Competition for space and resources is handled explicitly through confinement of cells on the matrix of automaton elements and through different glucose consumption rates for tumor and normal cells, rather than through the Lotka–Volterra competition parameters used in the continuum model. In the automaton model, the low pH-induced death of normal (and tumor) tissue saturates with increasing acid concentration (due to the use of thresholds in the automaton rules) rather than remaining proportional to acid concentration as in the continuum model. Acid removal and glucose delivery is through an actual vessel network rather than through *ad hoc* phenomenological terms in the differential equations of the reaction-diffusion model. Nevertheless, the two models do display some similarities in their growth dynamics and morphologies, at least qualitatively, in that both have an acid production threshold that must be exceeded in order for tumor invasion to progress and that they both display a hypocellular gap between the advancing tumor front and retreating normal tissue. The models differ significantly, however, in many other aspects of the tumor morphologies they predict. In the continuum model, the tumor is a homogeneous structure comprising either all tumor cells or a constant ratio of tumor to normal cells. As can be seen in Fig. 3, the automaton model displays varied tumor morphologies ranging from compact tumors to those with diffuse necrosis to those with regions of isolated necrosis to, finally, tumor cords or cuffs, all familiar to the pathologist.

Although some analytical results can be derived from the mean-field version of the automaton model [e.g. eqn (16)], the principal

‖‖ "Pushing" is something of a misnomer within the context of our model as stresses and strains suffered by a tumor during growth are not modeled. However, for an interesting treatment of this problem see Jones *et al.* (2000).

advantage of the reaction–diffusion model is that many results, including the tumor growth rate as a function of basic biological parameters, can be written as closed form mathematical expressions. Such expressions are not so useful for the quantitative results that can be derived from them, but rather what can be learned about the sensitivity of dependent quantities (such as the tumor growth rate or the extent of the acid gradient at the tumor–host interface) to the underlying basic biological parameters.

Our cellular automaton model of early tumor growth is quite versatile and extended studies may be performed by adding components to its state-vector and adding to the rule-set governing its evolution. In particular, variation of tumor and peritumor vascularity will be explicitly examined by allowing capillary destruction by tumor invasion and capillary creation by diffusing tumor generated angiogenesis factors such as VEGF. Introduction of oxygen in the model and its implications will be studied as well. Introduction of tumor cell phenotypic heterogeneity into the model may provide insight into clonal selection (Fidler & Hart, 1982; Fearson *et al*., 1987; Chang *et al*., 1995). The introduction of additional chemical fields of chemotherapeutic agents or biological modifiers will allow a more complete understanding of treatment strategies.

We also plan to implement a number of technical improvements in the simulation techniques. First, rather than the sharp thresholds currently used in the automaton rules, stochastic rules based on Michaelis–Menten-like distribution functions will be employed (at the expense of an additional parameter). Second, solutions of the full *time-dependent* differential equations will be obtained using operator splitting techniques, thus obviating the need for the adiabatic perturbation approximation introduced above. Third, periodic boundary conditions on the chemical fields at the system periphery will be replaced by their mean-field values [i.e. the solution of eqn (14) and its analog for each of the other chemical fields] at these locations. In this way, the effects of the "image tumors", which can be present at late time when the tumor has grown to an appreciable fraction of the system size, will be removed. Such effects usually manifest themselves as an artificial four-fold symmetry in the tumor morphology and chemical field distributions (see Fig. 3d in which a hint of such symmetry can be detected).

The authors would like to thank the referees for useful comments and Ms Dianne Fattig for help in preparing the manuscript.

REFERENCES

ABRAMS, H. L., SPIRA, R. & GOLDSTEIN, N. (1997). Metastases in carcinoma: analysis of 1000 autopsied cases. *Cancer*, 74–85.

ADAM, J. A. & BELLOMO, N., eds (1997). A Survey of Models for Tumor-immune System Dynamics. Boston: Birkhäuser.

ANDERSON, A. R. & CHAPLAIN, M. A. (1998). Continuous and discrete mathematical modes of tumor-induced angiogenesis. *Bull. Math. Biol.* **60,** 857–899.

BIERMAN, A. J., TARTOOLEN, L. G., DELAAT, S. W. & MOOLENAAR, W. H. (1987). The exchanger is constitutively activated in P19 embryonal carcinoma cells, but not in a differentiated derivative. Responsiveness to growth factors and other stimuli. *J. Biol. Chem.* **262,** 9621–9628.

BYRNE, H. M. & CHAPLAIN, M. A. (1995). Growth of nonnecrotic tumors in the presence of inhibitors. *Math. Biosci.* **130,** 151–181.

CASCIARI, J. J., OTIRCHOS, S. V. & SUTHERLAND, R. M. (1992). Variation in tumor growth rates and metabolism with oxygen concentration, glucose concentration, and extracellular pH. *J. Cell Physiol.* **151,** 386–394.

CHANG, K. W., LANCONI, S., MANGOLD, K. A., HUBCHAK, S. & SCARPELLI, D. G. (1995). Multiple genetic alterations in hamster pancreatic ductal adenocarcinomas. *Cancer Res.* **55,** 2560–2568.

CHAPLAIN, M. A. & ANDERSON, A. R. (1996). Mathematical modeling, simulation and prediction of tumor induced angiogenesis. *Invasion Metastasis* **16,** 222–234.

CRONE, C. & LEVITT, D. G. (1984). Capillary permeability to small solutes. In: *Handbook of Physiology*: *A critical, comprehensive presentation of physiological knowledge and concepts*, *Section* 2: *The Cardiovascular System*, Vol. IV: *Microcirculation*, *Part* 1 (Renkin, E. M. & Michel, C. C., eds), p. 414 and pp. 434–437. Bethesda, ML: American Physiological Society.

DAIRKEE, S. H., DENG, S. H., STAMPFER, M. R., WALDMAN, R. M. & SMITH, H. S. (1995). Selective cell culture of primary breast cancer. *Cancer Res.* **35,** 2516–2519.

DE GAETANO, A. & ARINO, O. (2000). Mathematical modeling of the intravenous glucose tolerance test. *J. Math. Biol.* **40,** 136–168.

DE RIESE, W., GOLDENBERG, K., ALLHOFF, E., STIEF, C., SCHLICK, R., LIEDKE, S. & JONAS, U. (1991). Metastatic renal cell carcinoma (RCC): spontaneous regression, long-term survival and late recurrence. *Int. Urol. Nephrol.* **23,** 13–25.

DÜCHTING, W. & VOGELSAENGER, T. (1984). Analysis, forecasting and control of three-dimensional tumor growth and treatment. *J. Med. Syst.* **8,** 461–475.

DÜCHTING, W. & VOGELSAENGER, T. (1985). Recent progress in modeling and simulation of three-dimensional tumor growth and treatment. *J. Med. Syst.* **8,** 461–475.

DURAND, R. E. (1983). Cellular oxygen utilization and radiation response of V-79 spheroids. *Adv. Exp. Med. Biol.* **159,** 419–434.

ERMENTROUT, G. B. & EDELSTEIN-KESHET, L. (1993). Cellular automata approaches to biological modeling. *J. theor. Biol.* **160,** 97–133.

FEARSON, E. R., HAMILTON, S. R. & VOGELSTEIN, B. (1987). Clonal analysis of human colorectal rumors. *Science* (Washington DC) **238,** 193–197.

FIDLER, I. J. & HART, I. R. (1982). Biological diversity in metastatic neoplasm: origins and implications. *Science* (Washington DC), **21,** 998–1003.

FOLKMAN, J., WATSON, K., INGBER, D. & HANAHAN, D. (1989). Induction of angiogenesis during the transition from hyperplasia to neoplasia. *Nature* (Lond.) **339,** 58–61.

FOLKMAN, J. (1992). The role of angiogenesis in tumor growth. *Cancer Biol.* **3,** 65–71.

GANONG, W. F. (1999). Review of Medical Physiology, 19th edn. Chapter 19, p. 329. New York: Appleton & Lange.

GARCIA TABAR, P. J., MONTOYA LIROLA, M. D., ETXEPARE, ARROSAGARAY, P., CASTILLO JIMENO, J. M., ACINAS GARCIA, O. & ALVAREZ MARTINEZ, J. (1992). Spontaneous disappearance of pulmonary metastasis secondary to renal cell carcinoma after nephrectomy. Presentation of a case and review of the literature. *Actas Urol. Esp.* **16,** 430–434.

GATENBY, R. A., KESSLER, H. B., ROSENBLUM, J. S., COIA, L. R., MOLDOFSKY, P. J., HARTZ, W. H. & BRODER, G. B. (1988). Oxygen distribution is squamous cell carcinoma metastases and its relation to the outcome of radiation therapy. *Int. J. Radiat. Oncol. Biol. Phys.* **14,** 831–838.

GATENBY, R. A. (1991). Population ecology issues in tumor growth. *Cancer Res.* **51,** 2542–2547.

GATENBY, R. A. (1995). The potential role of transformation-induced metabolic changes in tumor-host interaction. *Cancer Res.* **55,** 4151–4156.

GATENBY, R. A. & GAWLINSKI, E. T. (1996). A Reaction-Diffusion Model of Cancer Invasion. *Cancer Res.* **56,** 5745–5753.

GILLIES, R. J., LIU, Z. & BHUJWALLA, Z. (1994). 31P-MRS measurements of extracellular pH of tumors using 3-aminopropylphosphonate. *Am. J. Physiol.* **267,** C195–C203.

GRIFFITH, J. R. (1991). Are cancer cells acidic? *Br. J. Cancer* **64,** 425–427.

GULLINO, P. M., GRANTHAM, F. H., COURTNEY, A. H. & LOSONCZY, I. (1967). Relationship between oxygen and glucose consumption by transplanted tumors *in vivo*. *Cancer Res.* **27,** 1041–1052.

HARGUINDEY, S., HENDERSON, E. S. & NAEHER, C. (1979). Effects of systemic acidification of mice with Sarcoma 180. *Cancer Res.* **39,** 4364–4371.

HAWKINS, R. A., HOH, C., GLASPY, J., CHO, Y., DAHLBOM, M., REGE, S. & MESSA, C. (1992). The role of positron emission tomography in oncology and other whole-body applications. *Semin. Nucl. Med.* **22,** 268–284.

HELMLINGER, G., YUAN, F., DELLIAN, M. & JAIN, R. K. (1997). Interstitial pH and pO_2 gradients in solid tumors *in vivo*: high-resolution measurements reveal a lack of correlation. *Nat Med.* **2,** 177–182.

HOLASH, J., MAISONPIERRE, P. C., COMPTON, D., BOLAND, P., ALEXANDER, C. R., ZAGZAG, D., YANCOPOULOS, G. D. & WIEGAND, S. J. (1999). Vessel cooption, regression, and growth in tumors mediated by angiopoietins and VEGF. *Science* **284,** 1994–1998.

JABOUR, B. A., CHOI, Y., OOH, C. K., REGE, S. D., SOONG, J. L., LUFKIN, R. B., HANAFEE, W. M., MADDHI, J. & CHAIKEN, L. (1993). Extracranial head and neck tumors: PET imaging with 2-[F-18]-fluoro-2-deoxy-D-glucose. *Radiology* **186,** 27–35.

JACKSON, T. L. & BYRNE, H. M. (2000). A mathematical model to study the effects of drug resistance and vasculature on the response of solid tumors to chemotherapy. *Math. Biosci.* **164,** 17–38.

JONES, A. F., BYRNE, H. M., GIBSON, J. S. & DOLD, J. W. (2000). A mathematical model of the stress induced during avascular tumor growth. *J. Math. Biol.* **40,** 473–499.

KALLINOWSKI, F. & VAUPEL, P. (1988). pH distributions in spontaneous and isotransplanted rat tumours. *Br. J. Cancer* **58,** 314–321.

KALLINOWSKI, F., VAUPEL, P., RUNKEL, S., BERG, G., FORTMEYER, H. P., BAESSLER, K. H. & WAGNER, K. (1988). Glucose uptake, lactate release, ketone body turnover, metabolic micromilieu and pH distributions in human breast cancer xenografts in nude rats. *Cancer Res.* **48,** 7264–7272.

KANSAL, A. R., TORQUATO, S., HARSH, G. R., CHIOCCA, E. A. & DEISBOECK, T. S. (2000a). Simulated brain tumor growth dynamics using a three-dimensional cellular automaton. *J. theor. Biol.* **203,** 367–382.

KANSAL, A. R., TORQUATO, S., HARSH, G. R., CHIOCCA, E. A. & DEISBOECK, T. S. (2000b). Cellular automaton of idealized brain tumor growth dynamics. *BioSystems* **55,** 119–127.

KAPLAN, D. L. & BORON, W. F. (1994). Long-term expression c-H-ras stimulates Na–H and Na^+-H^4_T dependent Cl–HCO3 exchange in N1H-3T3 fibroblasts. *J. Biol. Chem.* **269,** 4116–4124.

KATO, Y., NAKAYAMA, Y., UMEDA, M. & MIYAZAKI, K. (1994). Induction of 103-kDa gelatinase type IV collagenase by acidic culture conditions in mouse metastatic melanoma cell lines. *J. Biol. Chem.* **267,** 11424–11430.

KLINGER, M. E. (1951). Secondary tumors of the genitourinary tract. *J. Urol.* **65,** 144–154.

KOIKE, H., YOSHIMOTO, T., TAKIUCHI, H., IHARA, H., ARIMA, M., MORI, Y. & IKOMA, F. (1990). A case of spontaneous disappearance of pulmonary metastasis of renal cell carcinoma following nephrectomy. *Hinyokika Kiyo*, **36,** 1443–1446.

KRATZ, A. & LEWANDROWSKI, K. B. (1998). Normal reference laboratory values. *N. Engl. J. Med.* **339,** 1063–1072.

KRAUS, M. & WOLF, B. (1996). Implications of Acidic Tumor Microenvironment for Neoplastic Growth and Cancer Treatment: A Computer Analysis. *Tumor Biol.* **17,** 133–154.

KRAUS, M. & WOLF, B. (1998). Physicochemical microenvironment as key regulator for tumor microevolution, invasion and immune response: targets for endocytotechnological approaches in cancer treatment. *Endocytobiosis Cell. Res.* **12,** 133–156.

LIU, X. H., KIRSCHENBAUM, A., YAO, S., SREARNS, M. E., HOLLAND, J. F., CLAFFEY, K. & LEVINE, A. C. (1999). Upregulation of vascular endothelial growth factor by cobalt chloride-simulated hypoxia is mediated by persistent induction of cyclooxybenase-2 in a metastatic human prostate cancer cell line. *Clin. Exp. Metastasis* **17,** 687–694.

MARKUS, M., BOHM, D. & SCHMICK, M. (1999). Simulation of vessel morphogenesis using cellular automata. *Math. Biosci.* **156,** 191–206.

MARTIN, G. R & JAIN, R. K. (1994). Noninvasive measurement of interstitial pH profiles in normal and neoplastic tissue using fluorescent ration imaging microscopy. *Cancer Res.* **54,** 5670–5674.

MARUŠIĆ, M., BAJZER, Ž., FREYER, J. P. & VUK-PAVLOVIĆ, S. (1994). Analysis of growth of multicellular tumor spheroids by mathematical models. *Cell Prolif.* **27,** 73–94.

MUELLER-KLIESER, & SUTHERLAND, R. M. (1982). Oxygen tension in multicell spheroids of two cell lines. *Br. J. Cancer* **45**(2)**,** 256–264.

MUELLER-KLIESER, W., WALENTA, S., PASCHEN, W., KALLINOWSKI, F. & VAUPEL, P. (1988). Metabolic imaging in micro-regions of tumors and normal tissues with bioluminescense and photon counting. *J. Natl Cancer Inst.* **80,** 842–848.

NEWSOME, J. E. & TULLOCK, W. S. (1966). Metastatic tumors in the kidney. *Br. J. Urol.* **38,** 1–6.

OLSEN, L., SHERRATT, J. A., MAINI, P. K. & ARNOLD, F. (1997). A mathematical model for the capillary endothelial cell-extracellular matrix interactions in wound-healing angiogenesis. *IMA J. Math. Appl. Med. Biol.* **14,** 261–281.

PATEL, A. A., LEMIEUX, S. K. & GATENBY, R. A. (1998). A cellular automaton model of tumor growth. Proceedings of the Association of University Radiologists, March 1998. p. 60.

PERUMPANANI, A. J. & NORBURY, J. (1999). Numerical interactions of random and directed motility during cancer invasion. *Math. Comput. Model.* **30,** 123–133.

PEZZELLA, F., PASTORINO, U., TAGLIABUE, E., ANDREOLA, S., GASPARINI, G., MENARD, S., GATTER, K. C., HARRIS, A. L., FOX, S., BUYSE, M., PILOTTI, S., PIEROTTI, M. & RILKE, F. (1997). Non-small-cell lung carcinoma tumor growth without morphological evidence of neo-angiogenesis. *Am. J. Pathol.* **151,** 1417–1423.

PRESS, W. H., TEUKOLSKY, S. A., VETTERLING, W. T. & FLANNERY, B. P. (1996). *Numerical Recipes in C*: *The Art of Scientific Computing*, 2nd edn, Section 19.5, pp. 863–871. New York: Cambridge University.

QI, A. S., ZHENG, X., DU, C. Y. & AN, B. S. (1993). A cellular automaton model of cancerous growth. *J. theor. Biol.* **161,** 1–12.

REW, D. A. & WILSON, G. D. (2000). Cell production rates in human tissues and tumours and their significance. Part II: clinical data. *Eur. J. Surg. Oncol.* **26,** 405–417.

ROZHIN, J., SAMENI, M., ZIEGLER, G. & SLOANE, B. F. (1994). Pericellular pH affects distribution and secretion of cathepsin B in malignant cells. *Cancer Res.* **54,** 6517–6525.

SHANT, K., ASHUR, G., CHENG, L., GED, B., NAJIB, H., JI, M. W. & NIGEL, B. (1999). Breast Carcinoma: Vascular Density Determined Using CD105 Antibody Correlates with Tumor Prognosis. *Cancer Res.* **59,** 856–861.

SLEEMAN, B. D., ANDERSON, A. R. & CHAPLAIN, M. A. (1999). A mathematical analysis of a model for capillary network formation in the absence of endothelial cell proliferation. *Appl. Math. Lett.* **12,** 121–127.

SMITH, T. A. (2000). Mammalian hexokinases and their abnormal expression in cancer. *Br. J. Biomed. Sci.* **57,** 170–178.

SMOLLE, J. (1998a). Fractal tumor stromal border in a nonequilibrium growth model. *Anal. Quant. Cytol. Histol.* **20,** 7–13.

SMOLLE, J. (1998b). Cellular automaton simulation of tumor growth—equivocal relationships between simulation parameters and morphologic pattern features. *Anal. Cell Pathol.* **17,** 71–82.

SMOLLE, J. & STETTNER, H. (1993). Computer simulation of tumor cell invasion by a stochastic growth model. *J. theor. Biol.* **160,** 63–72.

STUBBS, M., RODRIGUES, L., HOWE, F. A., WANG, J., JOONG, K. S., VEECH, R. & GRIFFIN, J. R. (1994). Metabolic consequences of a reversed pH gradient in rat tumors. *Cancer Res.* **54,** 4011–4016.

SHWEIKI, D., ITIN, A., SOFFER, D. & KESHET, E. (1992). Vascular endothelial growth factor induced by hypoxia may mediate hypoxia-initiated angiogenesis. *Nature* **359,** 843–845.

SHWEIKI, D., NEEMAN, M., ITIN, A. & KESHET, E. (1995). Induction of vascular endothelial growth factor expression by hypoxia and by glucose deficiency in multicell spheroids: implications for tumor angiogenesis. *Proc. Natl Acad. Sci. U.S.A.* **92**(3)**,** 768–772.

SUTHERLAND, R. M. & DURAND, R. E. (1976). Radiation response of multicell spheroids—an *in vitro* tumor model. *Curr. Top. Radiat. Q* **11**(1)**,** 87–139.

SUTHERLAND, R. M. & DURAND, R. E. (1984). Growth and cellular characteristics of multicell spheroids. *Recent Results Cancer Res.* **95,** 24–49.

TANNOCK, I. F. & ROTIN, D. (1989). Acid pH in tumors and its potential for therapeutic exploitation. *Cancer Res.* **49,** 4373–4384.

VAUPEL, P., KALLINOWSKI, F. & OKUNIEFF, P. (1989). Blood flow, oxygen and nutrient supply, and metabolic microenvironment of human tumors: a review. *Cancer Res.* **49,** 6449–6465.

WAGLE, D. G., MOORE, R. H. & MURPHY, G. P. (1975). Secondary carcinomas of the kidney. *J. Urol.* **114,** 30–32.

WALENTA, S., WETTERLING, M., LEHRKE, M., SCHWICKERT, G., SUNDFØR, ROFSTAD, E. & MUELLER-KLIESER, W. (2000). High lactate levels predict likelihood of metastases, tumor recurrence and restricted patient survival in human cervical cancers. *Cancer Res.* **60,** 916–921.

WARD, J. P. & KING, J. R. (1997). Mathematical modeling of avascular tumor growth. *IMA J. Math. Appl. Med. Biol.* **14,** 39–69.

WARD, J. P. & KING, J. R. (1999). Mathematical modeling of avascular tumor growth II: Modeling growth saturation. *IMA J. Math. Appl. Med. Biol.* **16,** 171–211.

WARBURG, O. (1930). *The metabolism of Tumors* (English translation by F. Dickens). London: Constable.

WOLFRAM, S. (1986). *Theory and Application of Cellular Automata.* Singapore: World Scientific.

YAMASAKI, H. (1991). Aberrant expression and function of gap junctions during carcinogenesis. *Environ. Health Perspect.* **93,** 191–197.

YONEKURA, Y., BENUA, R. S., & BRILL, A. B. (1982). Increased accumulation of 2-deoxy-2-[^{18}F]fluoro-D-glucose in liver metastases from colon cancer. *J. Nucl. Med.* **23,** 1133–1137.

YOSHINO, S. & WAKUI, M. (1988). Spontaneous regression of lung metastasis of renal cell carcinoma: a case report. *Hinyokika Kiyo* **34,** 2167–2169.

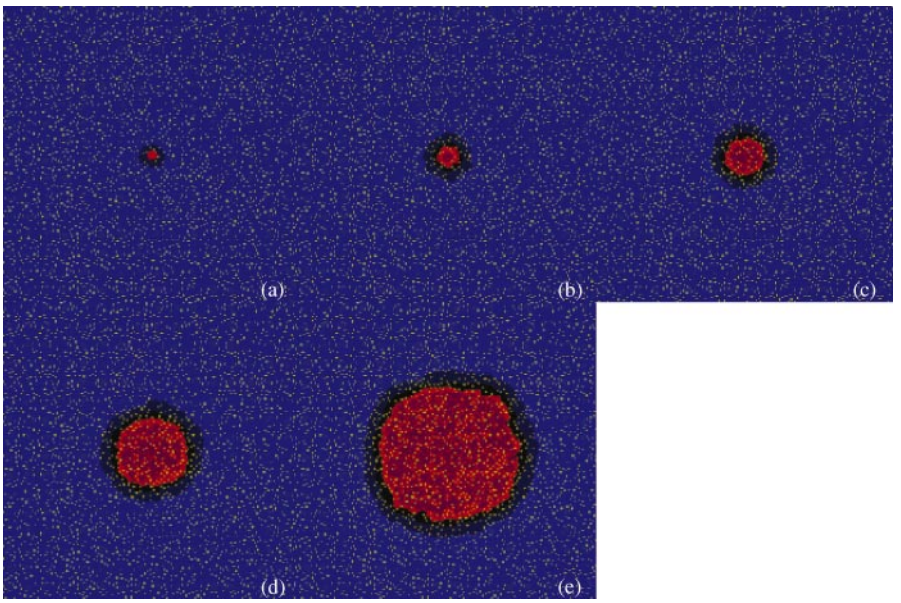

FIG. 2. The temporal evolution of a typical ($\phi_v = 0.08$, $\dot{H}_T^A = 3.0 \times 10^{-5}$ mM/s) tumor on a 200×200 matrix of automaton elements is shown at generations 1, 5, 10, 20 and 40 (A–E, respectively). Bright red elements are occupied by an active tumor cell, dark red by quiescent tumor, bright blue by active normal, dark blue by quiescent normal, and black elements by necrotic debris. By the fifth generation, a well-defined hypocellular gap (black) has formed before the advancing tumor front. By late time, the tumor is composed of an active ring surrounding a diffusely mixed core of active and quiescent tumor cells. The relative constancy of the widths of the active tumor ring, hypocellular gap and quiescent normal ring indicates that the tumor front is propagating as an invariant traveling wave (see text).

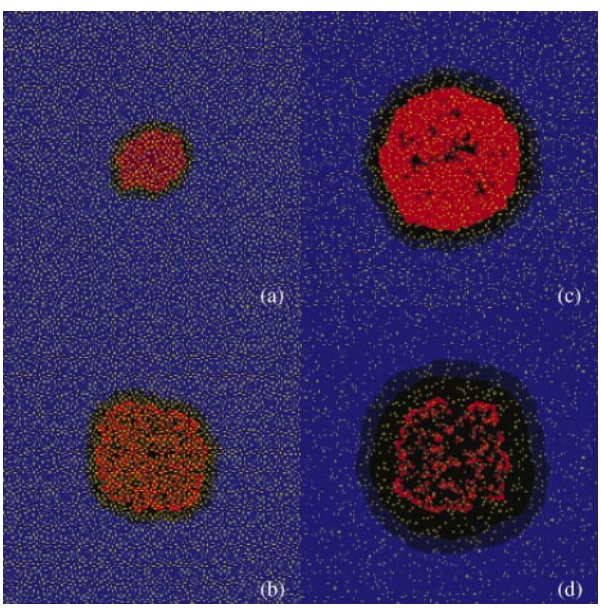

FIG. 3. A wide variety of tumor morphologies and dynamics can be obtained by varying the tumor phenotype and its vascular environment. Four different tumors that have been growing for the same amount of time (40 generations), each starting from the same initial size, are depicted. In both (a) and (b) $\phi_v = 0.18$ and $\dot{H}_T^A = 1.8 \times 10^{-4}$ mM/s, however in (a) tumor quiescence is admitted by setting $\mathrm{pH}_T^Q = 6.4$ and in (b) it is suppressed by setting $\mathrm{pH}_T^Q = \mathrm{pH}_T^D = 6.0$. Note that a growth rate enhancement has been obtained by the tumor in (b) at the expense of diffuse necrosis suffered throughout. In (c) the vessel density and acid production rate have been lowered to $\phi_v = 0.08$ and $\dot{H}_T^A = 3.0 \times 10^{-5}$ mM/s, respectively, while keeping tumor quiescence suppressed ($\mathrm{pH}_T^Q = 6.0$) resulting in necrosis confined to central cores. In (d) the vascularity is lowered further to $\phi_v = 0.04$ resulting in a tumor that initially grows but soon "self poisons", surviving only in cords around blood vessels. The late-time growth rates of tumors in (a)–(c) are constant while that of the tumor in (d) is decreasing. Presumably, the acquisition of additional blood supply by the tumor in (d) through neoangiogenesis would restore its aggressive growth.

doi:10.1006/jtbi.2001.2385